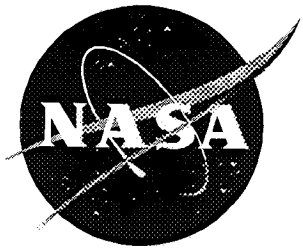

NASA Technical Paper 3472

Extension of the BRYNTRN Code to Monoenergetic Light Ion Beams

Francis A. Cucinotta and John W. Wilson
Langley Research Center • Hampton, Virginia

Francis F. Badavi
Christopher Newport University • Newport News, Virginia

National Aeronautics and Space Administration
Langley Research Center • Hampton, Virginia 23681-0001

November 1994

This publication is available from the following sources:

NASA Center for AeroSpace Information
800 Elkridge Landing Road
Linthicum Heights, MD 21090-2934
(301) 621-0390

National Technical Information Service (NTIS)
5285 Port Royal Road
Springfield, VA 22161-2171
(703) 487-4650

Introduction

Radiation transport models are required for the evaluation of risk to passengers and crews on high-altitude airplanes and to astronauts in low-Earth orbit or deep space and for understanding degradation properties of materials, including microelectronics, on orbiting satellites. Light ions such as ^{2}H or ^{4}He are present as primary and secondary radiations in solar and galactic cosmic rays. Light ion beams also are useful in radiotherapy treatment of cancer patients. (See refs. 1 and 2.) In nuclear reactions the mass dependence of secondary radiations results in broader distributions of secondary energies for lighter mass particles. Several mechanisms (direct knockout, evaporation, coalescence, etc.) will produce light products of nuclear collisions and lead to a wider distribution of secondary energies. The broad spectrum of light ion secondaries leads to some different approaches to solution of the Boltzmann equation for radiation transport compared with heavy ion transport. (See ref. 3.) The heavy fragments in nuclear reactions are usually spectators in that they receive only small momentum and energy transfer.

In this report, we discuss the modifications of the monoenergetic version of the BRYNTRN transport code (refs. 4–6) for the transport of light ion beams. Validation of radiation transport methods must include monoenergetic beams and a continuous spectrum of primary radiations. The BRYNTRN transport code solves the Boltzmann equation in the straight-ahead approximation using the method of characteristics developed in references 3–6. Recently we developed an energy-dependent model of light ion nuclear interaction cross sections. (See refs. 7 and 8.) The previous monoenergetic version of the BRYNTRN code considered only the coupled proton-neutron transport problem. Here we discuss the extension of the BRYNTRN code to include the database for transport of the light ion beams ^{2}H(d), ^{3}H(t), ^{3}He(h), and ^{4}He(α). The BRYNTRN code previously calculated target fragmentation effects through local energy deposition. We also describe an equilibrium target fragment field that was added to consider the effects of fragments on the linear energy transfer (LET) spectrum.

Symbols

A	mass number
A_T	mass number of target
c	speed of light, fm/sec
D	dose, cGy
d	^{2}H
E	particle energy, MeV/amu
E'	$= \varepsilon(r')$
E_0	beam kinetic energy, MeV/amu
E_{0j}	average energy of target fragment j
F	defined in equation (15)
$\overline{F}$	defined in equation (14)
$f_{jk}(E, E')$	differential energy cross section for redistribution of particle type and energy
h	^{3}He
m	nucleon mass, MeV/c^2
R	nuclear matter radii, fm
r	residual range, g/cm^2
$S(E)$	proton-stopping power, MeV/(g/cm^2)
t	^{3}H
x	depth of material, g/cm^2
Z	charge
z	distance, g/cm^2
α	alpha particle
δ	Dirac delta function
δ_{Jk}	Kronecker delta
$\varepsilon(r)$	energy associated with r, MeV/amu
$\zeta_j(r,t)$	defined in equation (7)
ν_j	range-scaling parameter
σ	cross section, mb
$\sigma_j(E)$	total cross section, mb
Φ	linear energy transfer, MeV/cm
$\phi_j(x,E)$	differential flux spectrum of type j ions
ψ_j	scaled flux
Subscripts:	
EL	elastic recoils
j, k	ions of type j and k
n	neutron
T	target

Boltzmann Equations and Solutions

The propagation of high-energy nuclei and their secondaries through bulk matter is described by the Boltzmann equation, which in the straight-ahead approximation (refs. 5 and 6) is of the form

$$\left[\frac{\partial}{\partial x} - \nu_j \frac{\partial}{\partial E} S(E) + \sigma_j(E)\right] \phi_j(x,E) = \sum_k \int_0^\infty f_{jk}(E,E')\phi_k(x,E')\,dE' \tag{1}$$

where ν_j denotes the range-scaling parameter equal to Z_j^2/A_j, Z is the charge, and A is the mass number. In equation (1), $S(E)$ is the proton-stopping power, $\sigma(E)$ is the total cross section, $\phi_j(x,E)$ is the differential flux spectrum of type j ions, and $f_{jk}(E,E')$ is a differential energy cross section for redistribution of particle type and energy.

Utilizing the definitions

$$r = \int_0^E \frac{dE'}{S(E')} \tag{2}$$

$$\psi_j(x,r) = S(E)\phi_j(x,E) \tag{3}$$

and

$$\overline{f}_{jk}(r,r') = S(E) f_{jk}(E,E') \tag{4}$$

we can rewrite equation (1) as

$$\left[\frac{\partial}{\partial x} - \nu_j \frac{\partial}{\partial r} + \sigma_j(r)\right] \psi_j(x,r) = \sum_k \int_r^\infty \overline{f}_{jk}(r,r')\psi_k(x,r')\,dr' \tag{5}$$

which is solved by Wilson et al. (refs. 5 and 6) as

$$\begin{aligned}\psi_j(x,r) = {} & \exp[-\zeta_j(r,x)]\psi_j(0,r+\nu_j x) \\ & + \sum_k \int_0^x \int_r^\infty \exp[-\zeta_j(r,z)]\overline{f}_{jk}(r+\nu_j z, r')\psi_k(x-z,r')\,dr'\,dz\end{aligned} \tag{6}$$

where the exponential is the integrating factor given by

$$\zeta_j(r,t) = \int_0^t \sigma_j(r+\nu_j t')\,dt' \tag{7}$$

Next we present the basis of numerical procedures for propagation of the solution at $\psi_j(x,r)$ to $\psi_j(x+h,r)$. Choosing h to be small such that

$$\sigma_j(r')h \ll 1 \tag{8}$$

then from perturbation theory (ref. 4) we derive

$$\psi_k(x+h-z,r') \approx \exp[-\zeta_k(r',h-z)]\psi_k[x,r'+\nu_k(h-z)] \tag{9}$$

For monoenergetic particle beams, the initial beam of type J particles of energy E_0 is

$$\psi_j(0,r) = \delta_{jJ}\delta(r_0 - r) \tag{10}$$

where $r_0 = R(E_0)$. The separation of the singular terms in the solution is written by the replacement

$$\psi_j(x,r) \rightarrow \psi_{j0}(x,r) + \psi_j(x,r) \tag{11}$$

Based on equations (8)–(11), the solution (refs. 3 and 7) at $x + h$ is

$$\psi_j(x+h,r) \approx \exp[-\zeta_j(r,h)]\psi_j(x_j, r+\nu_j h) + \sum_k \exp\left\{-\left[\zeta_j\left(r,\frac{h}{2}\right)+\zeta_k\left(r,\frac{h}{2}\right)\right]\right\}\left\{\overline{F}_{jk}\left(r,\nu_j h, r'_{0j}\right)\exp\left[-\zeta_k\left(r'_{0j}\right),h\right]\delta_{Jk} + \overline{F}_{jk}\left[r,\nu_j h, r+(\nu_k+\nu_j)\frac{h}{2}\right]\int_{r_k+(\nu_j h/2)+(\nu_k h/2)}^{\infty} dr'\,\psi_k(x,r')\right\} \tag{12}$$

for charged-particle propagation, where $r'_{0j} = r_0 - \nu_j[x + (h/2)]$, and

$$\psi_n(x+h,r) \approx \exp[-\zeta_n(r,h)]\psi_n(x,r) + h\sum_k\left(\exp\left\{-\left[\zeta_n\left(r,\frac{h}{2}\right)+\zeta_k\left(r'_0\frac{h}{2}\right)\right]\right\}\overline{f}_{nk}(r,r'_{0k})\exp[-\zeta(r'_{0k},x)]\delta_{Jk} + \int_r^{\infty} dr'\,\exp\left\{-\left[\zeta_n\left(r,\frac{h}{2}\right)+\zeta_k\left(r',\frac{h}{2}\right)\right]\right\}\overline{f}_{nk}(r,r')\psi_k\left(x,r'+\nu_k\frac{h}{2}\right)\right) \tag{13}$$

for neutron propagation. In equation (12) $\overline{F}$ is related to the cumulative spectrum F as

$$\overline{F}_{ij}(r,\nu_j h,r') = \int_0^h \overline{f}_{ij}(r+\nu_j z, r')\,dz \equiv F_{ij}(r+\nu_j h, r') - F_{ij}(r,r') \tag{14}$$

with

$$F_{ij}(r,r') = \int_0^{\varepsilon(r)} f_{ij}(E,E')\,dE \tag{15}$$

where $\varepsilon(r)$ is the energy associated with the residual range r and $E' = \varepsilon(r')$.

The numerical representation of particle ranges and stopping powers in the BRYNTRN code has been described in reference 6, where the database for proton and neutron nuclear interactions is also described. The database for light ion interactions is described in references 8 and 9. We note that the projectile-like fragments are represented by a Gaussian spectrum with energy-dependent width and downshift from the beam velocity. We expect that a sum of several Gaussian terms would more accurately represent these spectra. (See ref. 10.) The quasi-elastic events for light ions are represented by an approximation to the first collision term of the inelastic scattering series. (See ref. 11.)

Secondary Flux From Light Ion Beams

In figures 1 and 2, we show the secondary charged particle spectra at several depths in water for monoenergetic ^{4}He beams at 200 and 1000 MeV/amu, respectively. Two sources of secondary particles are clearly seen in the figures that correspond to a high-energy flux from projectile-like fragments and a low-energy flux from target-like fragments. The projectile-like fragments are produced at energies above that of the beam due to the internal Fermi motion of the nuclear-bound state. For the beam at 200 MeV/amu and for great depths, the projectile- and target-like secondaries overlap as the beam energy degrades and the secondaries slow from atomic interactions. A similar comparison is shown in figures 3 and 4 for aluminum shielding. In figures 1–4, the greater range of ^{3}H compared with ^{3}He is apparent.

In figures 5 and 6, we show the secondary proton spectra for monoenergetic ^{2}H beams at several depths in aluminum for 200 and 1000 MeV/amu, respectively. The pickup reactions for ^{2}H projectiles have not been included at this time, and no projectile-like secondaries with $Z > 1$ are included. Before discussing depth-dose curves and the LET spectrum for light ion beams, we next describe an equilibrium field of heavy target fragments of mass number $A_F > 4$.

Equilibrium Field of Target Fragments

The nuclear secondaries produced from the target atoms with $A_F > 4$ have average energies of only a few MeV or less and, therefore, are of extremely short range. Previously, their effects had been included only as locally deposited energy. (See ref. 6.) Consideration of the target fragmentation effects in the LET spectrum and of the radiation response quantities other than energy deposition requires an equilibrium field of target fragments. The differential flux for these ions can be solved in closed form (ref. 6) as

$$\phi_j(x,E;E_k) = \frac{1}{S_j(E)} \sum_k \int_E^\infty f_{kj}(E',E_k)\phi_k(x,E_k)\,dE' \tag{16}$$

where $\phi_k(x,E_k)$is a projectile-like ion k with energy E_k at x, which produces a target fragment j with energy E. The production spectrum from fragmentation is assumed of the form

$$f_{kj}(E,E_k) = \frac{\sigma_j \rho_T}{\left(2\pi E_{0j}^3\right)^{1/2}} \sqrt{E} \exp\left(\frac{-E}{2E_{0j}}\right) \tag{17}$$

where ρ_T is the density of the target material, σ_j is the microscopic fragmentation cross section, and E_{0j} is the average target fragment energy. The parameters σ_j and E_{0j} used in the BRYNTRN code are described in reference 6. Using equation (17) in equation (16), we find

$$\phi_j(x,E;E_k) = \frac{\sigma_j(E_k)\rho_T}{S_j(E)} \phi_k(E_k,x) \left[Erfc\left(\sqrt{\frac{E}{2E_{0j}}}\right) - \frac{2}{\sqrt{\pi}} \sqrt{\frac{E}{2E_{0j}}} \exp\left(\frac{-E}{2E_{0j}}\right)\right] \tag{18}$$

where $Erfc$ is the complementary error function. For composite materials, a summation over the target constituents is implied in equation (17). The energy spectrum of elastic recoils (ref. 6) is approximated by

$$f_{kj}(E,E_k) = \sigma_{\mathrm{EL}} \rho_T \frac{C_{\mathrm{EL}} \exp(-C_{\mathrm{EL}}E)}{1 - \exp[-C_{\mathrm{EL}}(1-D_{\mathrm{EL}})E_k]} \tag{19}$$

where σ_{EL} is the elastic scattering cross section and $C_{\mathrm{EL}} = A_T mc^2[B + (a^3/3)]$, where A_T is the mass number of the target, m is the nucleon mass, B is an average nucleon-nucleon slope parameter, and a is the target radius parameter. The energy transfer to the recoil is restricted by

$$0 \le E \le (1 - D_{\mathrm{EL}})E_k \tag{20}$$

with

$$D_{\mathrm{EL}} = \frac{(A_T - 1)^2}{(A_T + 1)^2} \tag{21}$$

The flux of recoils is then

$$\phi_j(x,E;E_k) = \frac{\rho_T \sigma_{\mathrm{EL}}}{S_j(E)} \frac{\{\exp(-C_{\mathrm{EL}}E) - \exp[-C_{\mathrm{EL}}(1-D_{\mathrm{EL}})E_k]\}}{1 - \exp[-C_{\mathrm{EL}}(1-D_{\mathrm{EL}})E_k]} \phi_k(x,E_k) \tag{22}$$

The equilibrium field of target fragments is found as

$$\overline{\phi}_j(x,E) = \int \phi_j(x,E;E_k)\,dE_k \tag{23}$$

For calculations, the production cross sections from light ions are assumed to scale to the nucleon-induced ones by the factor $A_k^{0.4}$. (See ref. 3.) An energy grid of 100 points with a maximum energy of 30 MeV/amu is used to obtain convergence of the equilibrium target fragment fields for water. Interface effects at the boundary of two media could be described in a similar manner as followed here and as described in reference 12.

Depth-Dose Curves for Monoenergetic Beams

In figures 7–9, we show calculations of absorbed dose versus depth in water shields for monoenergetic light ion beams at several energies. These figures provide a breakdown of the contributions from primaries (dotted line), secondary protons (dash-dot line), and all other secondaries (dashed line). Included in the secondary contribution are the contributions from heavier target fragments ($A_F > 4$) as described earlier. The increase in secondary contributions to the absorbed dose is apparent when the proton beam is compared with the heavier beams where projectile fragmentation provides additional particles. The ^{2}H range is about twice that of the proton; therefore, nuclear reactions can continue, which is also apparent in figures 7–9. The absorbed dose does not effectively represent harmful biological components of a radiation field, so we next consider the LET spectrum, which is more useful.

LET Spectrum for Monoenergetic Beams

The LET spectrum is closely related to the response of microdosimeters and provides a rough indication of biologically harmful components of a radiation field. Wilson and Badavi (ref. 13) have discussed the numerical treatment of the singularities in the transformation of energy spectra to LET spectra. We use this method to consider the LET spectrum in water for monoenergetic light ion beams and all nuclear secondaries from target fragmentation.

In figure 10(a), the LET spectrum from a 200-MeV proton beam is shown at various depths in water. A similar comparison is provided in figures 10(b) and 10(c) for a 200 MeV/amu, ^{2}H and ^{4}He beam, respectively. The inclusion of the heavy component of the target fragments ($A_F > 4$) provides particles above 200 keV/μm with significant numbers at the greater depths. The spikes in figures 10 and 11 occur both at a LET value corresponding to the peak in a Bragg ionization curve and near the LET value corresponding to minimal ionization for each charge group. The biological effectiveness of these ions is not a unique function of LET because biological effectiveness also depends on ion velocity due to thindown effects where the range of secondary electrons becomes small compared with the size of relevant damage sites inside cells. (See ref. 14.) In figures 11(a)–11(c), calculations of the LET flux spectrum at 1000 MeV/amu are shown. The high LET components increase compared with the 200 MeV/amu beams in figures 10(a)–10(c) due to more predominant nuclear fragmentation effects.

A similar comparison for the integral LET spectra is shown in figures 12(a)–12(c) and 13(a)–13(c).

Conclusion

The monoenergetic version of the BRYNTRN transport computer code has been extended to the transport of light ion beams (^{2}H, ^{3}H, ^{3}He, and ^{4}He). Illustrative calculations of energy spectrum, depth-dose curves, and LET spectrum were presented and discussed. The extensions described here will allow transport methods for space radiations to be validated through comparisons with laboratory experiments that involve light ion beams.

NASA Langley Research Center
Hampton, VA 23681-0001
August 16, 1994

References

1. Lyman, John T.; and Howard, Jerry: Dosimetry and Instrumentation for Helium and Heavy Ions. *Int. J. Radiat. Oncol. Biol. Phys.*, vol. 3, 1977, pp. 81–85.

2. Castro, Joseph R.; and Reimers, Monica M.: Charged Particle Radiotherapy of Selected Tumors in the Head and Neck. *Int. J. Radiat. Oncol. Biol. Phys.*, vol. 14, 1988, pp. 711–720.

3. Wilson, J. W.; Townsend, L. W.; Shinn, J. L.; Cucinotta, F. A.; Costen, R. C.; Badavi, F. F.; and Lamkin, S. L.: Galactic Cosmic Ray Transport Methods: Past, Present, and Future. *Adv. Space Res.*, vol. 14, no. 10, 1994, pp. (10)841–(10)852.

4. Wilson, John W.; and Lamkin, Stanley L.: Perturbation Theory for Charged-Particle Transport in One Dimension. *Nucl. Sci. & Eng.*, vol. 57, no. 4, Aug. 1975, pp. 292–299.

5. Wilson, John W.; Townsend, Lawrence W.; Nealy, John E.; Chun, Sang Y.; Hong, B. S.; Buck, Warren W.; Lamkin, S. L.; Ganapol, Barry D.; Khan, Ferdous; and Cucinotta, Francis A.: *BRYNTRN: A Baryon Transport Model.* NASA TP-2887, 1989.

6. Wilson, John W.; Townsend, Lawrence W.; Schimmerling, Walter; Khandelwal, Govind S.; Khan, Ferdous; Nealy, John E.; Cucinotta, Francis A.; Simonsen, Lisa C.; Shinn, Judy L.; and Norbury, John W.: *Transport Methods and Interactions for Space Radiations.* NASA RP-1257, 1991.

7. Lamkin, S. L.; Khandelwal, G. S.; Shinn, J. L.; and Wilson, J. W.: Numerical Methods for High Energy Nucleon Transport. *Proceedings of the Topical Meeting on New Horizons in Radiation Protection and Shielding*, American Nuclear Soc., Inc., 1992, pp. 165–170.

8. Cucinotta, Francis A.; Townsend, Lawrence W.; and Wilson, John W.: *Description of Alpha-Nucleus Interaction Cross Sections for Cosmic Ray Shielding Studies.* NASA TP-3285, 1993.

9. Cucinotta, Francis A.: *Calculations of Cosmic-Ray Helium Transport in Shielding Materials.* NASA TP-3354, 1993.

10. Cucinotta, F. A.: *Multiple-Scattering Model for Inclusive Proton Production in Heavy Ion Collisions.* NASA TP-3470, 1994.

11. Cucinotta, Francis A.; Townsend, Lawrence W.; and Wilson, John W.: Multiple-Scattering Effects in Quasi-elastic α-^{4}He Scattering. *Phys. Rev. C*, 3rd ser., vol. 46, no. 4, Oct. 1992, pp. 1451–1456.

12. Cucinotta, Francis A.; Hajnal, Ferenc; and Wilson, John W.: Energy Deposition at the Bone-Tissue Interface From Nuclear Fragments Produced by High-Energy Nucleons. *Health Phys.*, vol. 59, no. 6, Dec. 1990, pp. 819–825.

13. Wilson, John W.; and Badavi, Francis F.: *A Study of the Generation of Linear Energy Transfer Spectra for Space Radiations.* NASA TM-4410, 1192.

14. Katz, R.; Dunn, D. E.; and Sinclair, G. L.: Thindown in Radiobiology. *Radiat. Prot. Dosim.*, vol. 13, no. 1–4, 1985, pp. 281–284.

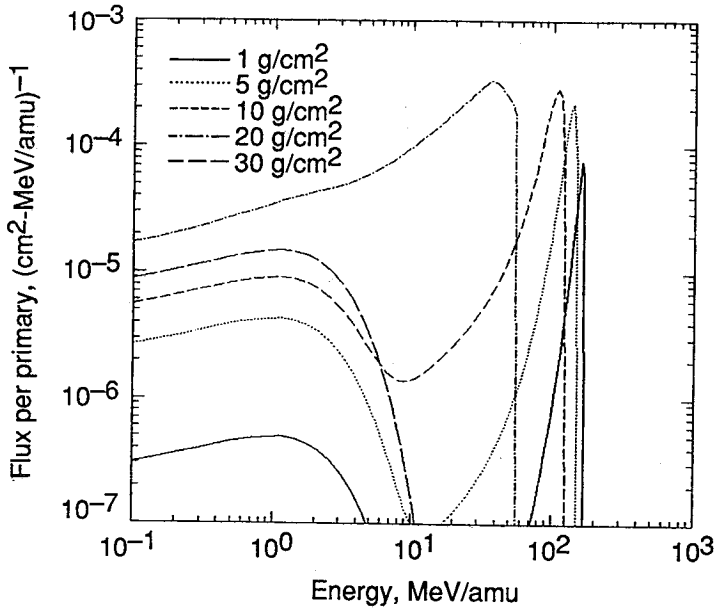

(a) Alpha emissions.

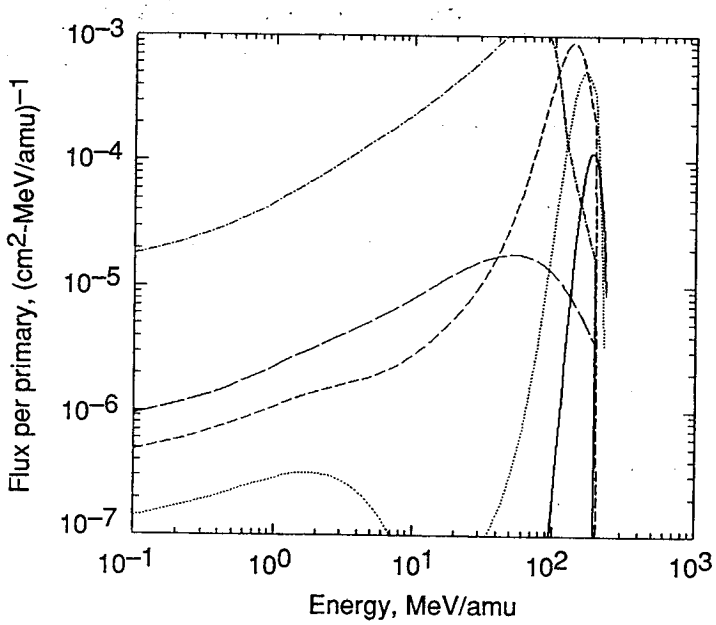

(b) Helion emissions.

Figure 1. Calculations of light ion flux spectrum in water shields from primary ^{4}He beam at 200 MeV/amu.

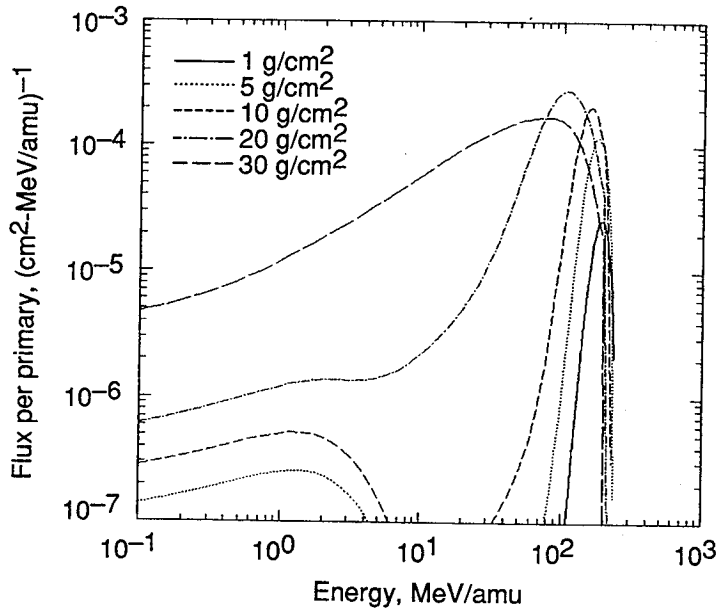

(c) Triton emissions.

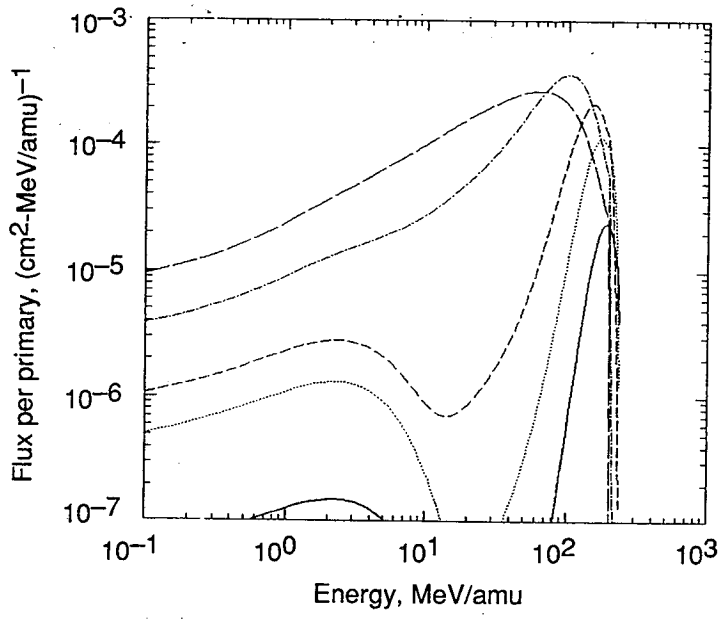

(d) Deuteron emissions.

Figure 1. Continued.

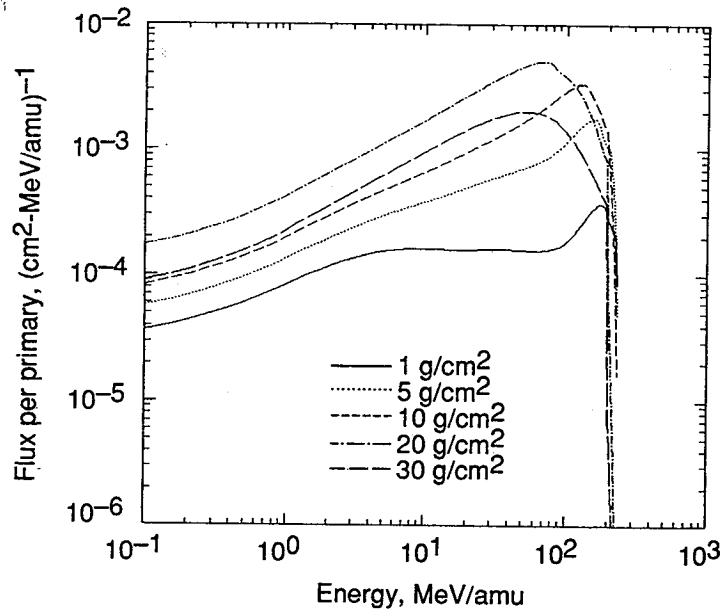

(e) Proton emissions.

Figure 1. Concluded.

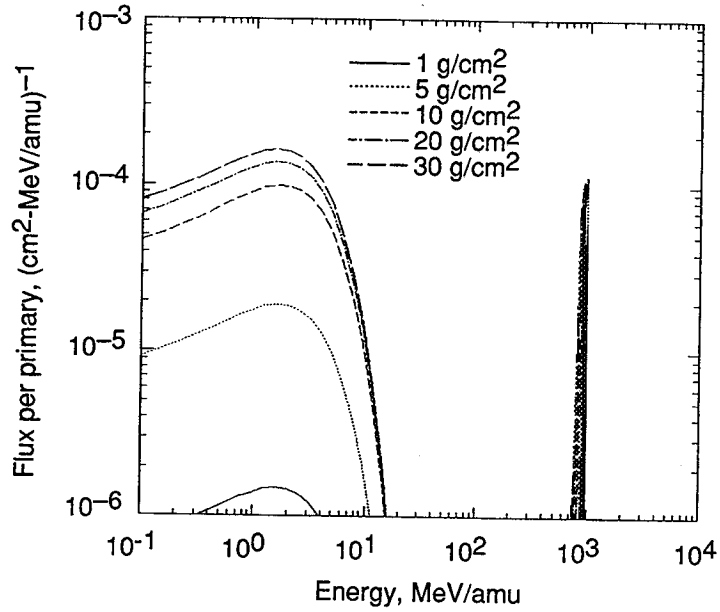

(a) Alpha emissions.

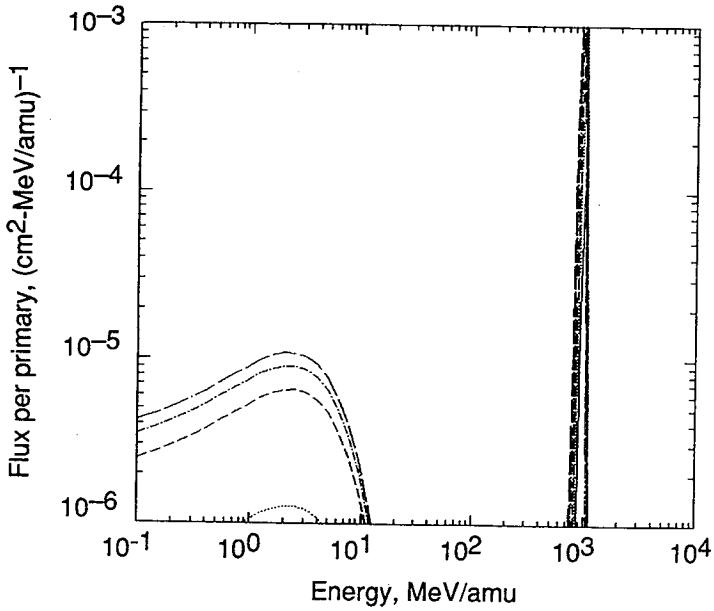

(b) Helion emissions.

Figure 2. Calculations of light ion flux spectrum in water shields from primary ^{4}He beam at 1000 MeV/amu.

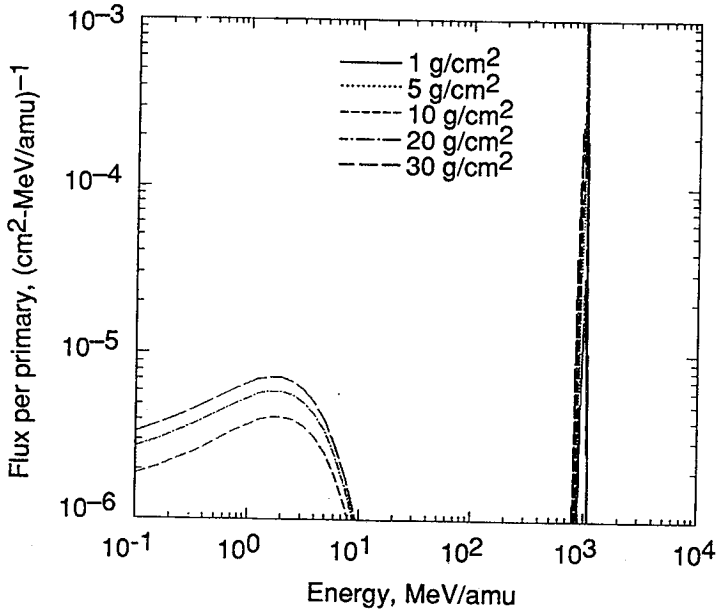

(c) Triton emissions.

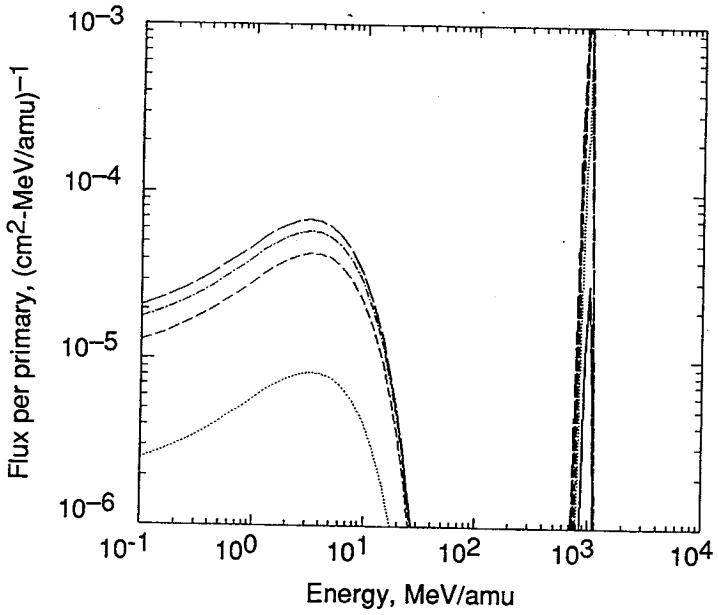

(d) Deuteron emissions.

Figure 2. Continued.

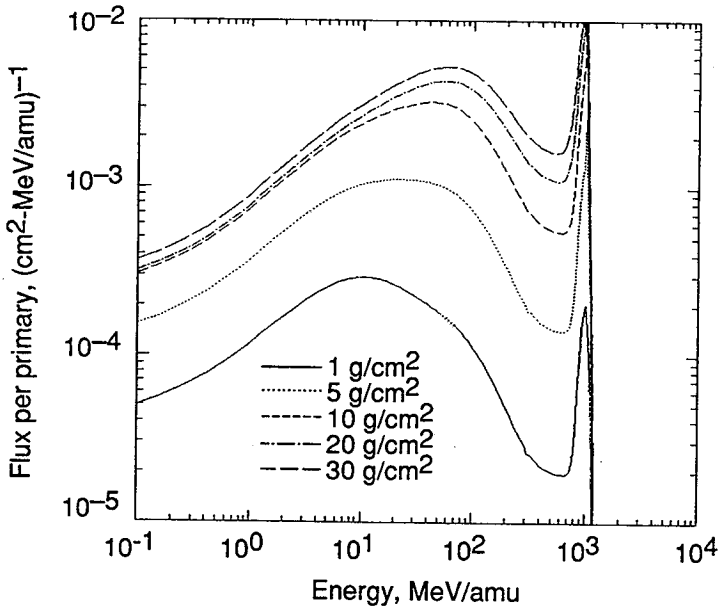

(e) Proton emissions.

Figure 2. Concluded.

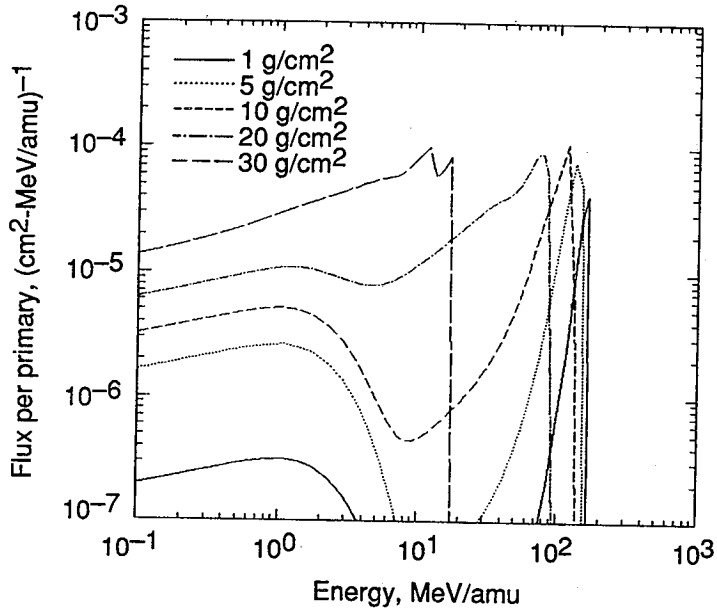

(a) Alpha emissions.

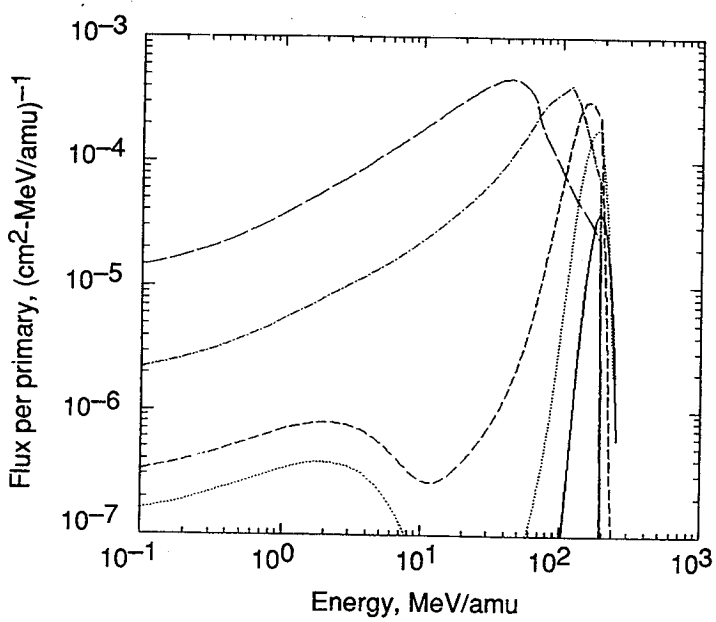

(b) Helion emissions.

Figure 3. Calculations of light ion flux spectrum in aluminum shields for primary ^{4}He beam at 200 MeV/amu.

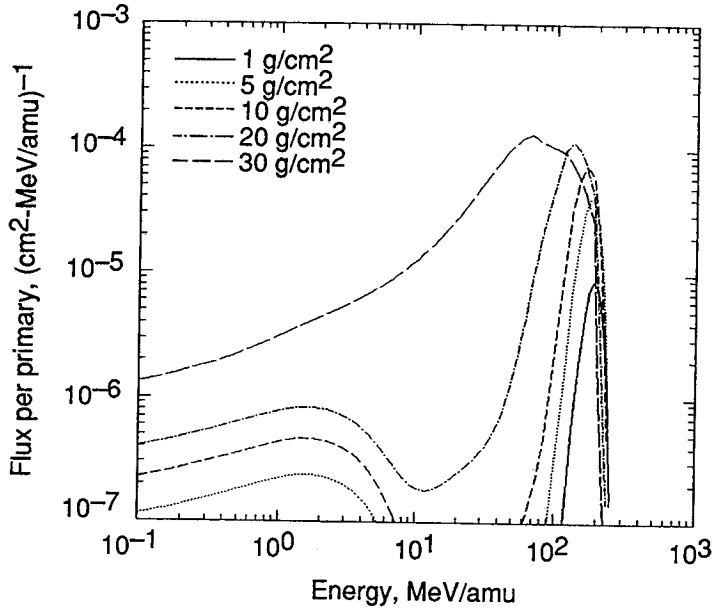

(c) Triton emissions.

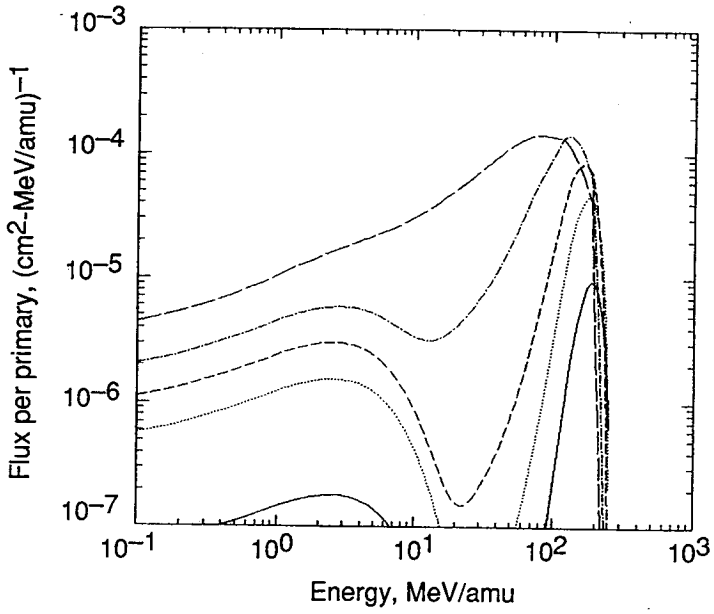

(d) Deuteron emissions.

Figure 3. Continued.

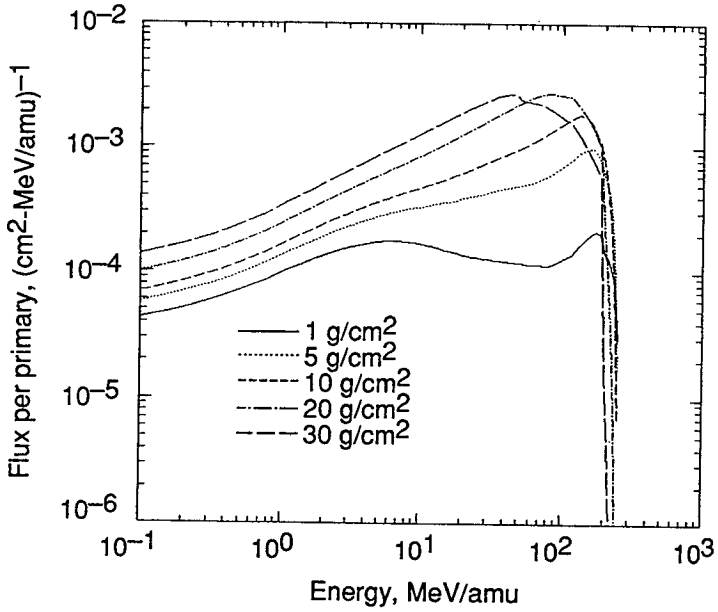

(e) Proton emissions.

Figure 3. Concluded.

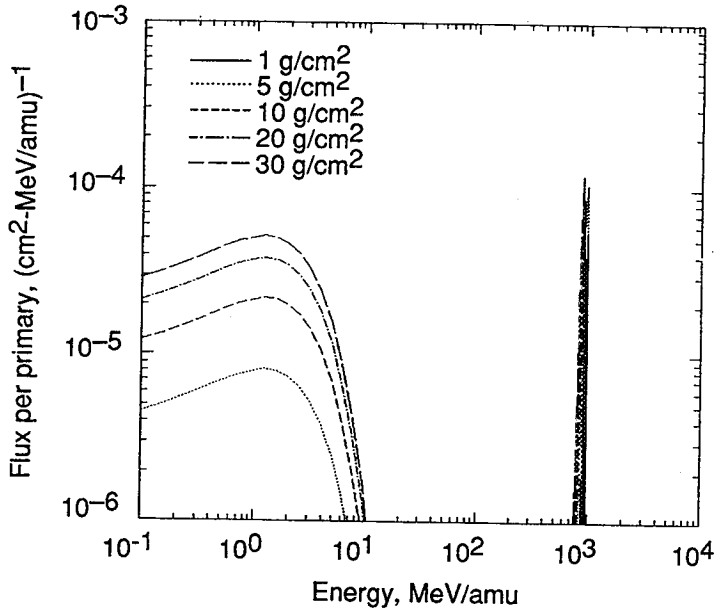

(a) Alpha emissions.

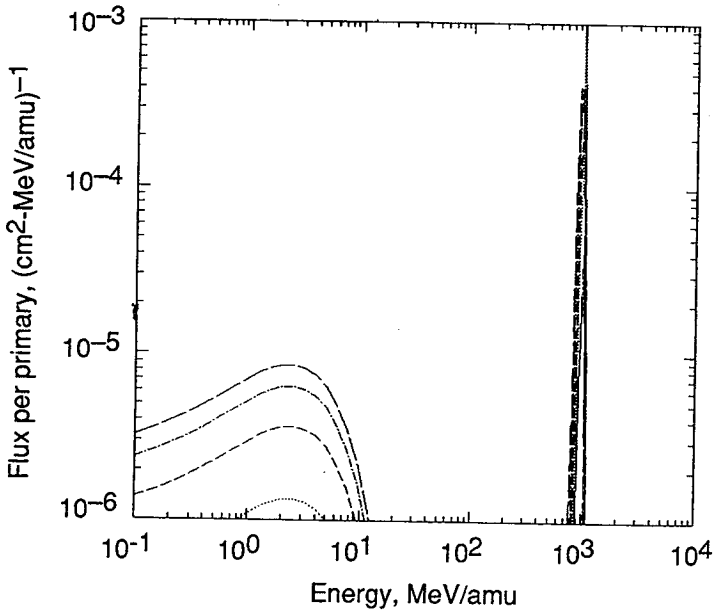

(b) Helion emissions.

Figure 4. Calculations of light ion flux spectrum in aluminum shields for primary ^{4}He beam at 1000 MeV/amu.

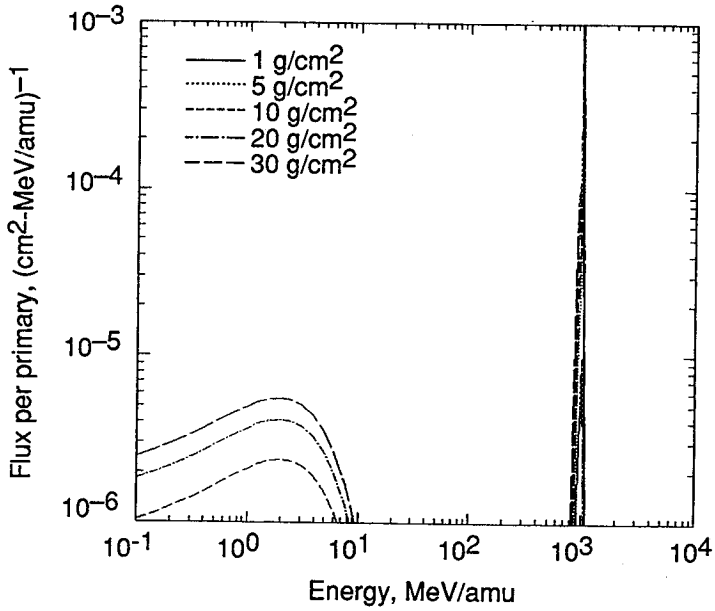

(c) Triton emissions.

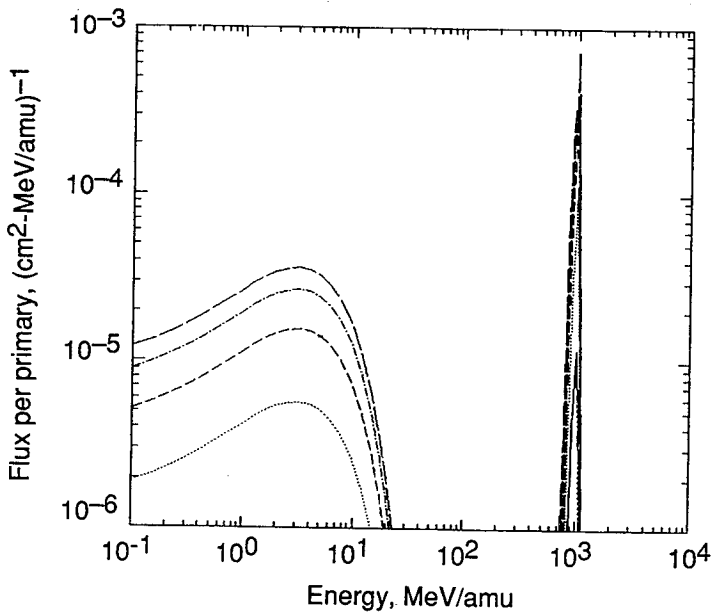

(d) Deuteron emissions.

Figure 4. Continued.

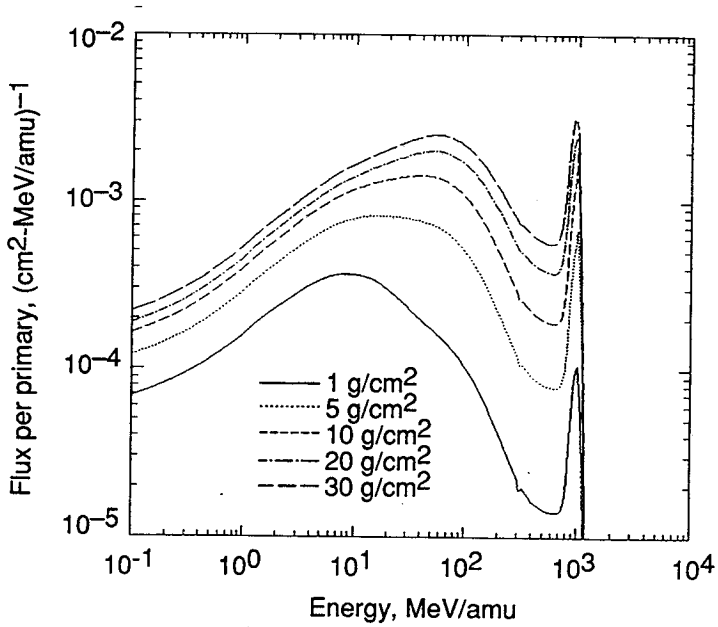

(e) Proton emissions.

Figure 4. Concluded.

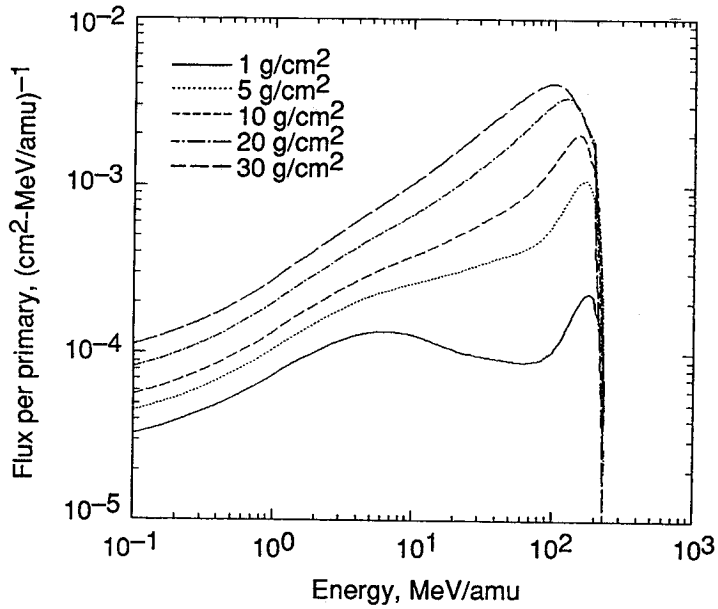

Figure 5. Calculations of proton flux spectrum in water shields from primary ^{2}H beam at 200 MeV/amu.

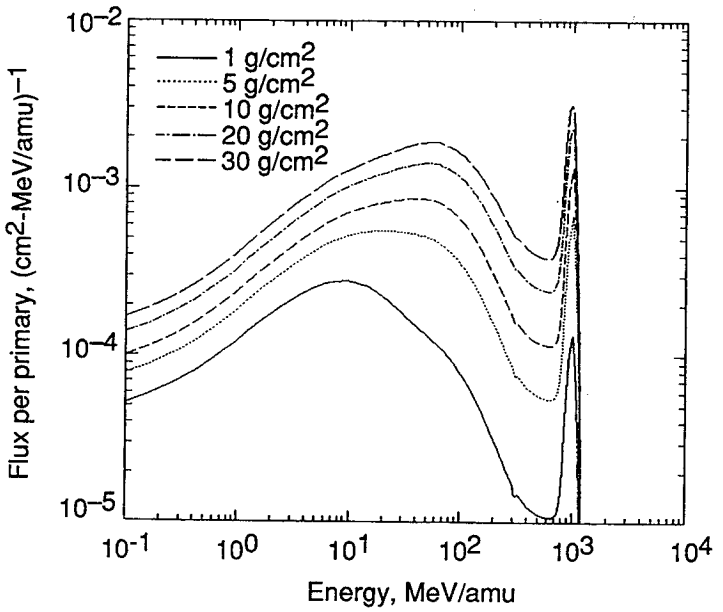

Figure 6. Calculations of proton flux spectrum in water shields from primary ^{2}H beam at 1000 MeV/amu.

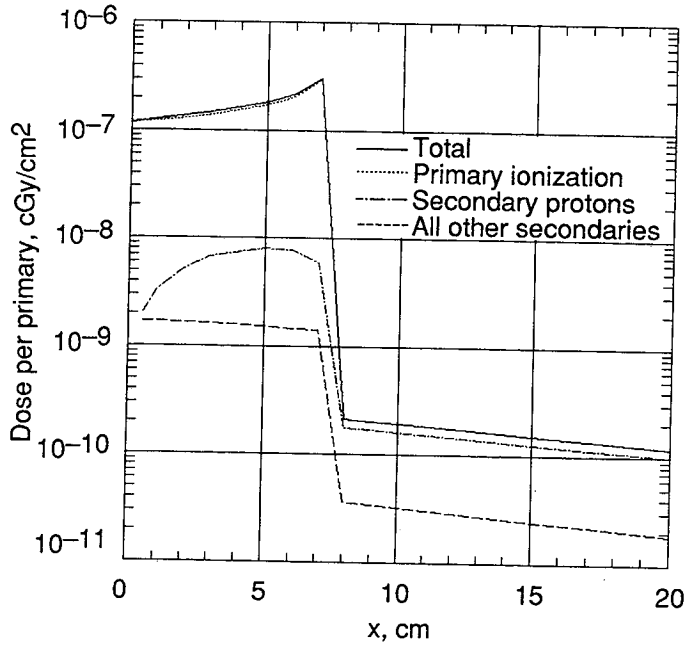

(a) Proton beam.

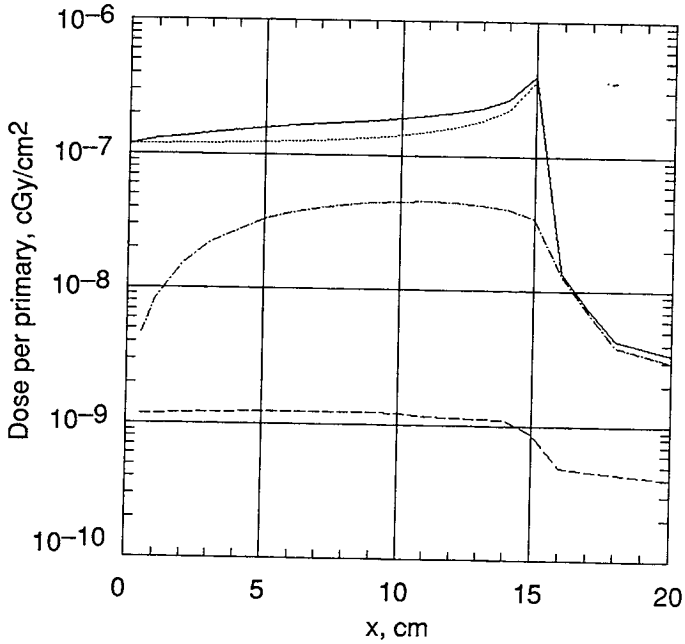

(b) ^{2}H beam.

Figure 7. Depth-dose curves for beams at 100 MeV/amu in water.

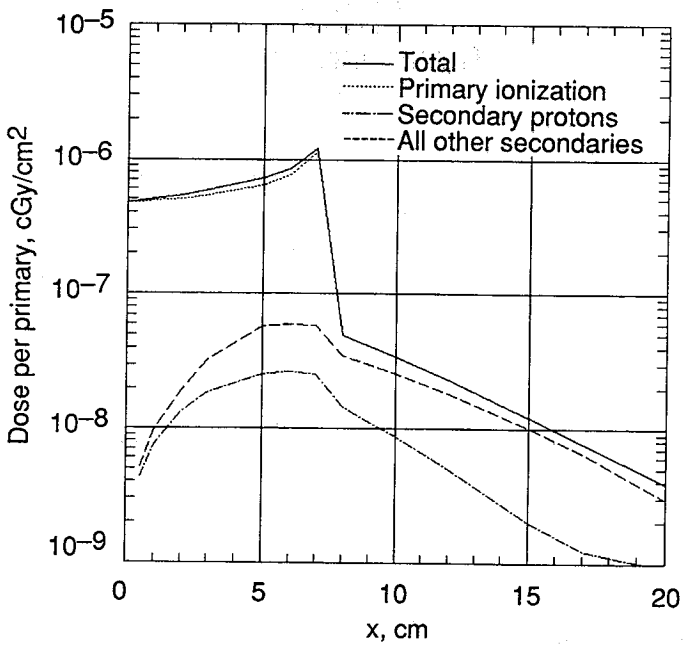

(c) ^{4}He beam.

Figure 7. Concluded.

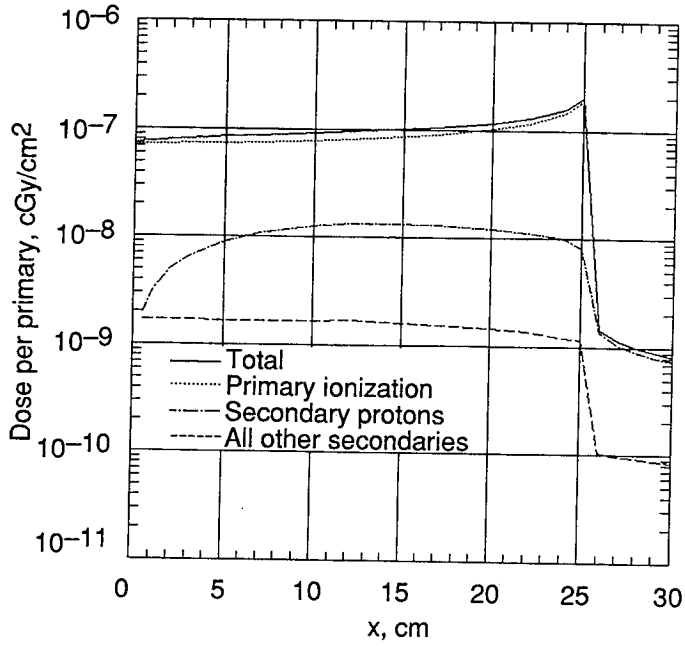

(a) Proton beam.

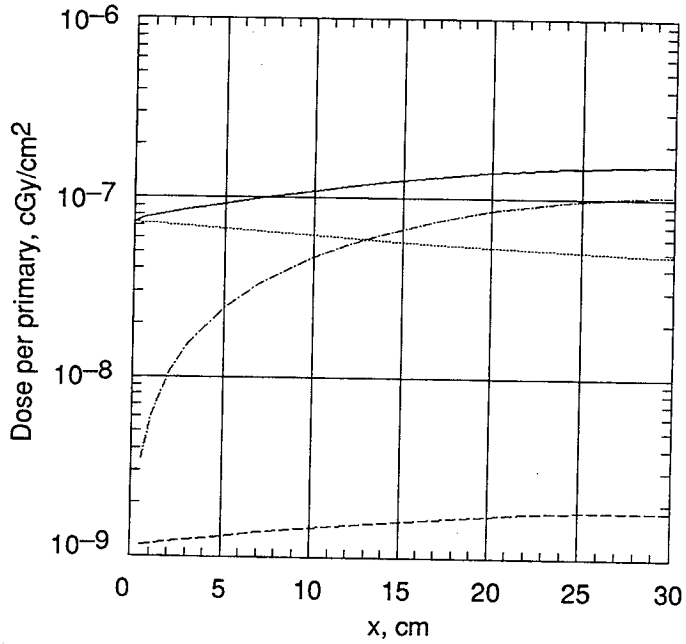

(b) ^{2}H beam.

Figure 8. Depth-dose curves for beams at 200 MeV/amu in water.

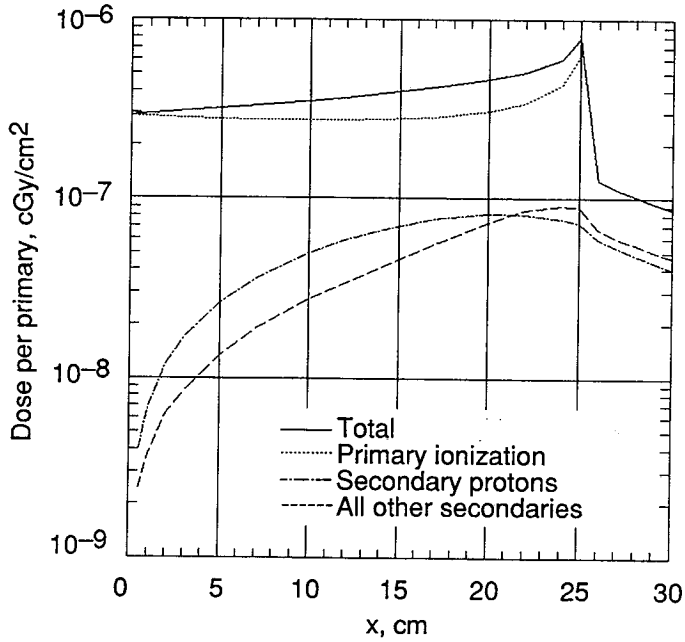

(c) ^{4}He beam.

Figure 8. Concluded.

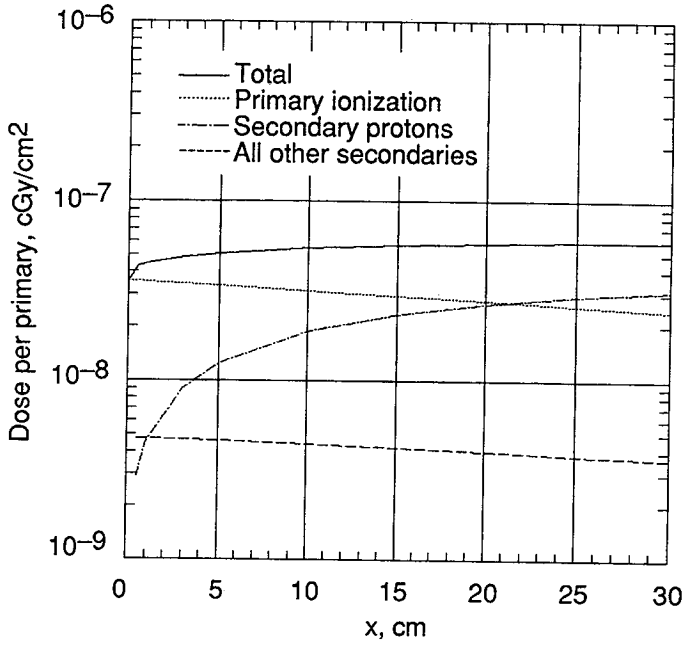

(a) Proton beam.

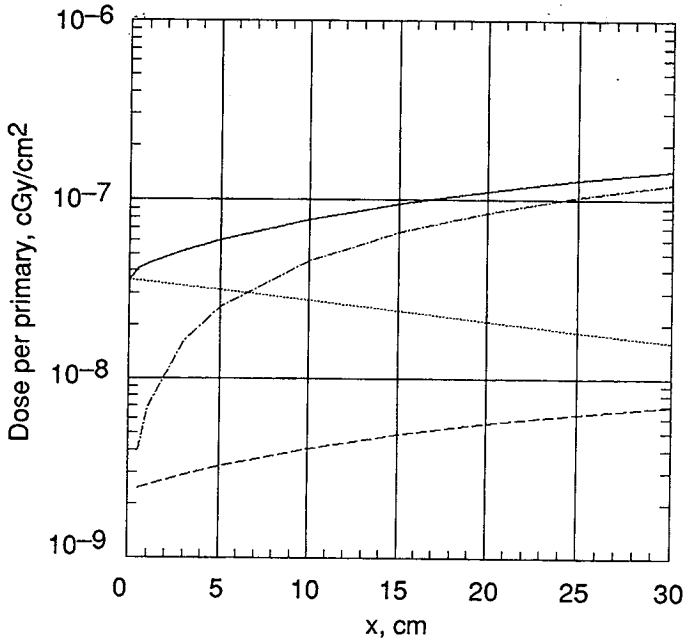

(b) ^{2}H beam.

Figure 9. Depth-dose curves for beams at 1000 MeV/amu in water.

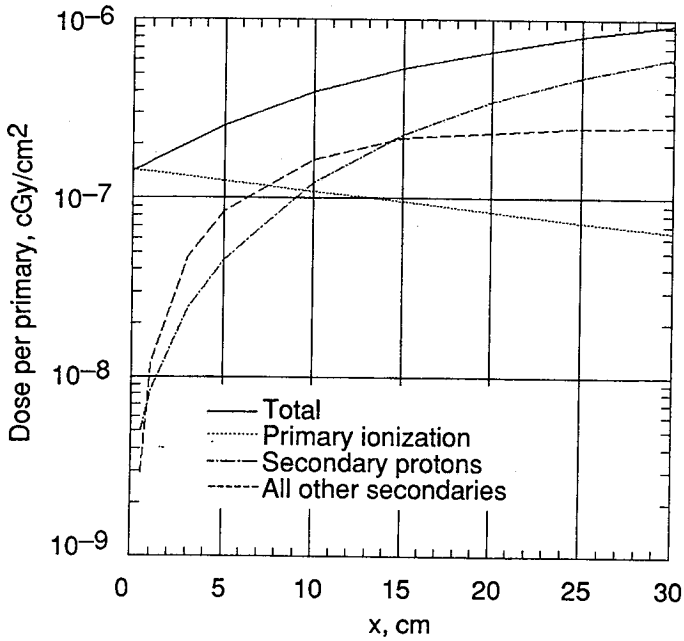

(c) ^{4}He beam.

Figure 9. Concluded.

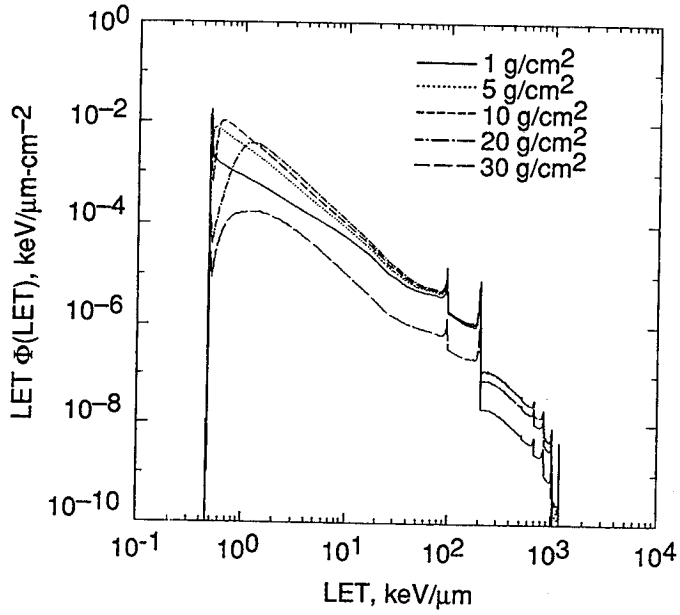

(a) Proton beam.

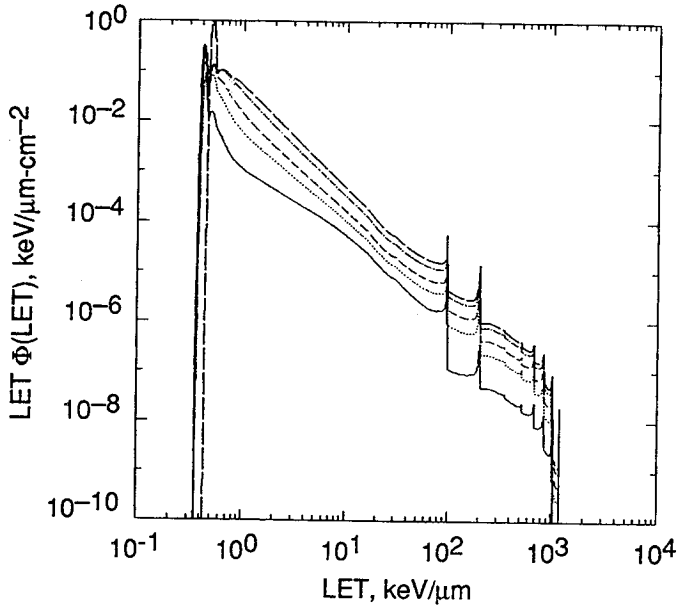

(b) ^{2}H beam.

Figure 10. Differential LET flux spectrum for beams at 200 MeV/amu and several depths in water.

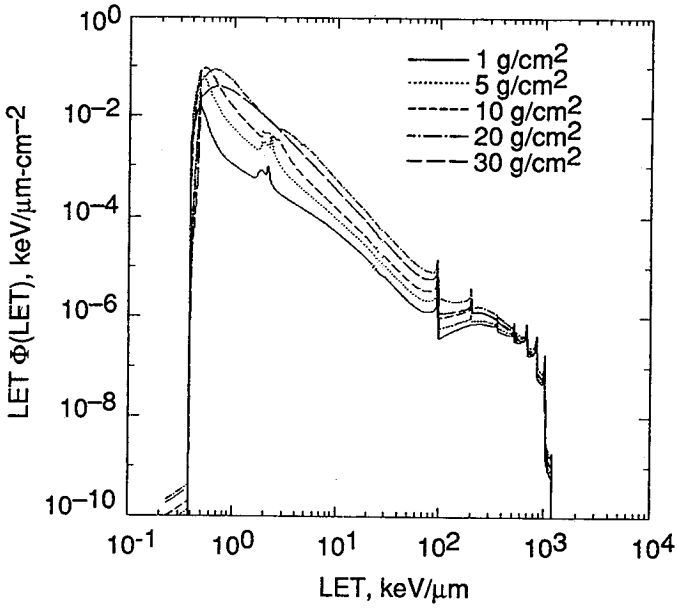

(c) ^{4}He beam.

Figure 10. Concluded.

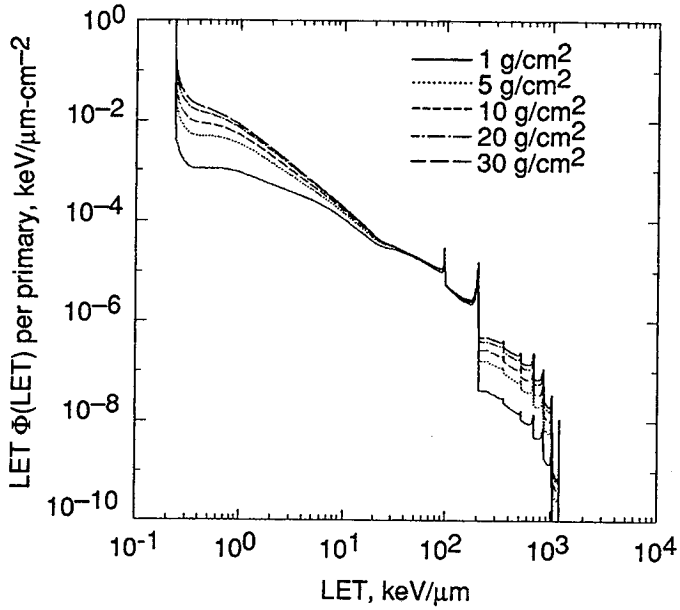

(a) Proton beam.

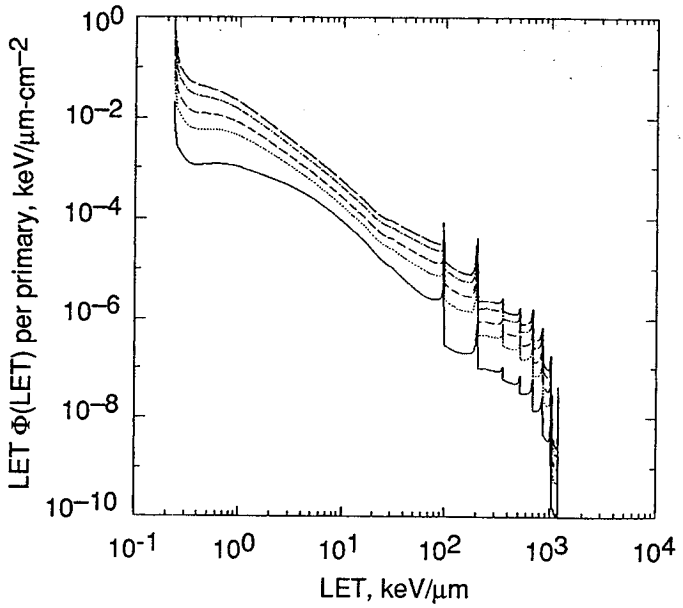

(b) ^{2}H beam.

Figure 11. Differential LET flux spectrum for beams at 1000 MeV/amu and several depths in water.

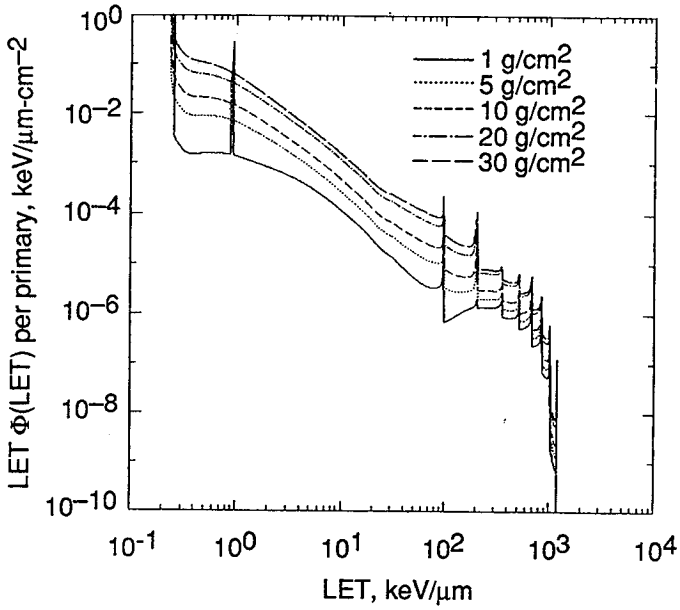

(c) ^{4}He beam.

Figure 11. Concluded.

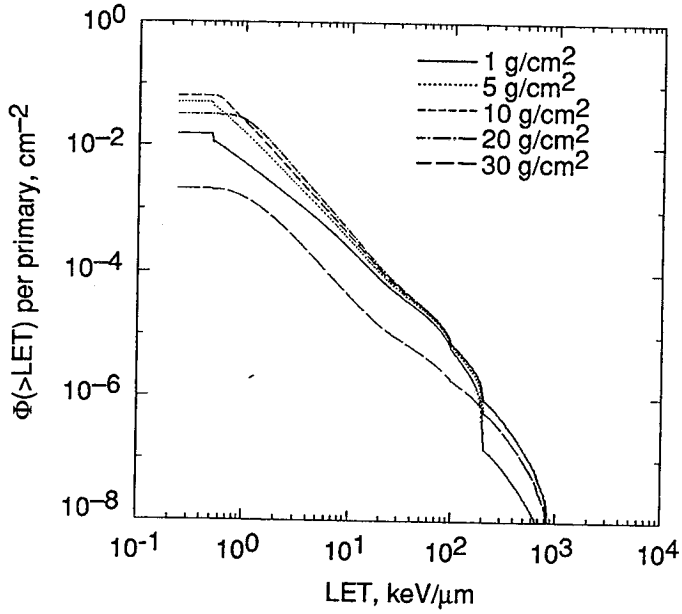

(a) Proton beam.

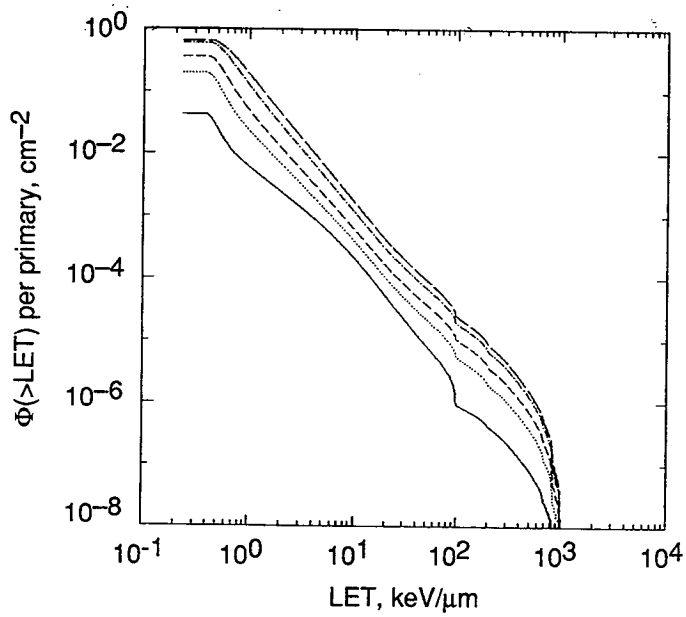

(b) ^{2}H beam.

Figure 12. Integral LET flux for beams at 200 MeV/amu and several depths in water.

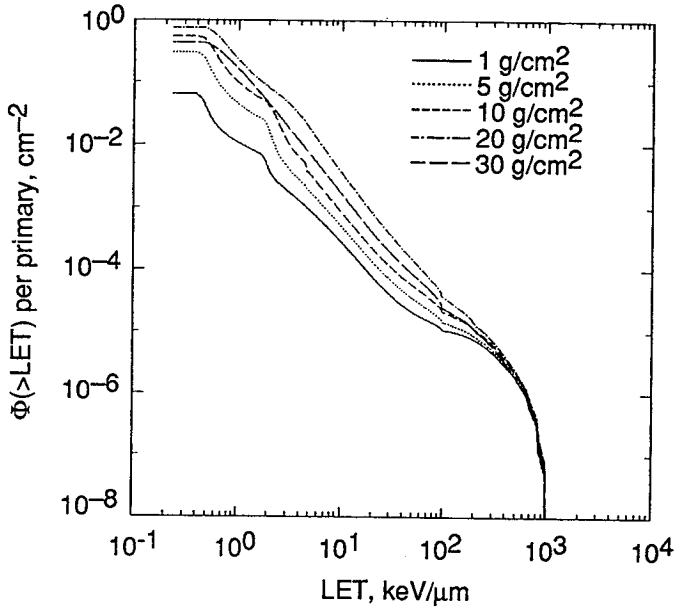

(c) ^{4}He beam.

Figure 12. Concluded.

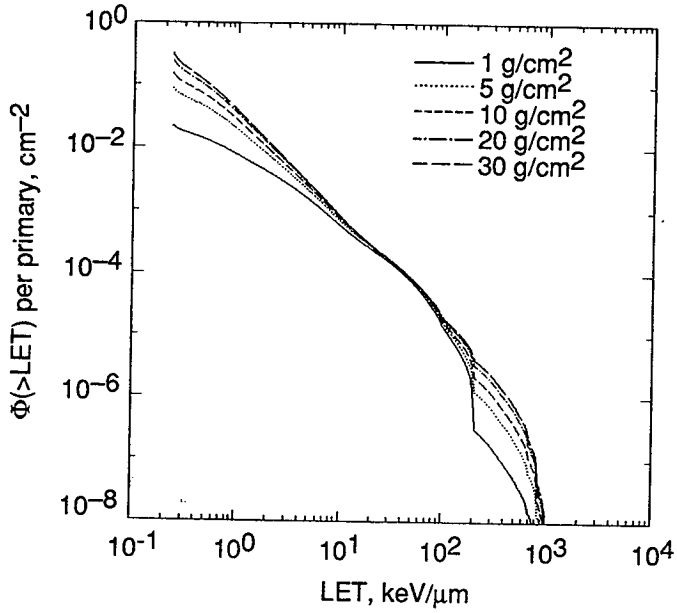

(a) Proton beam.

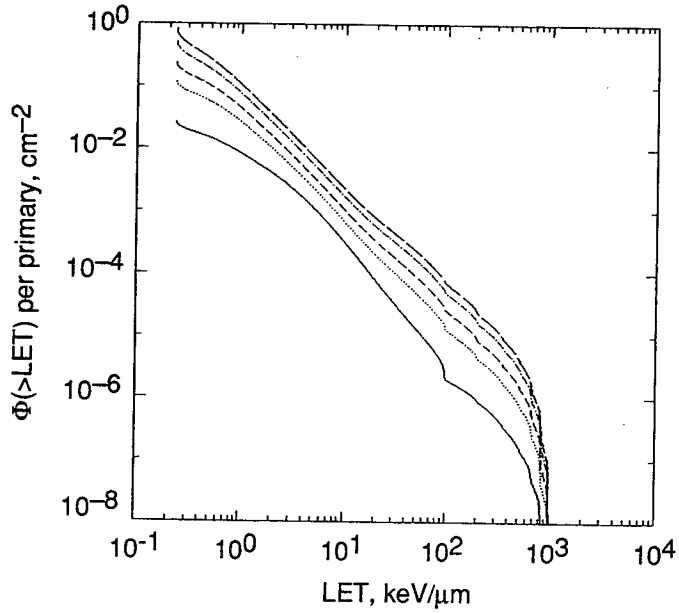

(b) ^{2}H beam.

Figure 13. Integral LET flux for beams at 1000 MeV/amu and several depths in water.

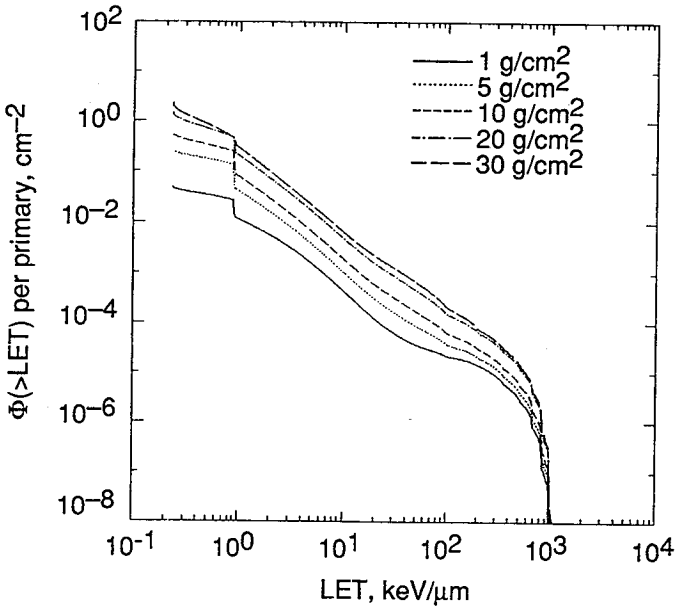

(c) ^{4}He beam.

Figure 13. Concluded.

REPORT DOCUMENTATION PAGE

Form Approved
OMB No. 0704-0188

1. AGENCY USE ONLY *(Leave blank)*

2. REPORT DATE
November 1994

3. REPORT TYPE AND DATES COVERED
Technical Paper

4. TITLE AND SUBTITLE
Extension of the BRYNTRN Code to Monoenergetic Light Ion Beams

5. FUNDING NUMBERS
WU 199-45-16-11

6. AUTHOR(S)
Francis A. Cucinotta, John W. Wilson, and Francis F. Badavi

7. PERFORMING ORGANIZATION NAME(S) AND ADDRESS(ES)
NASA Langley Research Center
Hampton, VA 23681-0001

8. PERFORMING ORGANIZATION REPORT NUMBER
L-17394

9. SPONSORING/MONITORING AGENCY NAME(S) AND ADDRESS(ES)
National Aeronautics and Space Administration
Washington, DC 20546-0001

10. SPONSORING/MONITORING AGENCY REPORT NUMBER
NASA TP-3472

11. SUPPLEMENTARY NOTES
Cucinotta and Wilson: Langley Research Center, Hampton, VA; Badavi: Christopher Newport University, Newport News, VA.

12a. DISTRIBUTION/AVAILABILITY STATEMENT
Unclassified–Unlimited

Subject Category 93

12b. DISTRIBUTION CODE

13. ABSTRACT *(Maximum 200 words)*
A monoenergetic version of the BRYNTRN transport code is extended to beam transport of light ions (^{2}H, ^{3}H, ^{3}He, and ^{4}He) in shielding materials (thick targets). The redistribution of energy in nuclear reactions is included in transport solutions that use nuclear fragmentation models. We also consider an equilibrium target-fragment spectrum for nuclei with mass number greater than four to include target fragmentation effects in the linear energy transfer (LET) spectrum. Illustrative results for water and aluminum shielding, including energy and LET spectra, are discussed for high-energy beams of ^{2}H and ^{4}He.

14. SUBJECT TERMS
Radiation transport; Cosmic rays; Radiotherapy

15. NUMBER OF PAGES
34

16. PRICE CODE
A03

17. SECURITY CLASSIFICATION OF REPORT	18. SECURITY CLASSIFICATION OF THIS PAGE	19. SECURITY CLASSIFICATION OF ABSTRACT	20. LIMITATION OF ABSTRACT
Unclassified	Unclassified	Unclassified	